

# Chaotic and frequency-locked atomic population oscillations between two coupled Bose-Einstein condensates

Chaohong Lee,<sup>1,\*</sup> Wenhua Hai,<sup>2</sup> Lei Shi,<sup>1</sup> Xiwen Zhu,<sup>1</sup> and Kelin Gao<sup>1</sup>

<sup>1</sup>*Laboratory of Magnetic Resonance and Atomic and Molecular Physics, Wuhan Institute of Physics and Mathematics, The Chinese Academy of Sciences, Wuhan 430071, Peoples Republic of China*

<sup>2</sup>*Department of Physics, Hunan Normal University, Changsha 410081, Peoples Republic of China*

(Received 21 March 2001; revised manuscript received 4 June 2001; published 2 October 2001)

We have investigated the chaotic and frequency-locked population oscillations between two coupled Bose-Einstein condensates with time-dependent asymmetric potential and damping. Under the deterministic perturbation, there exist stable oscillations close to the separatrix solution, which are Melnikov chaotic. Numerical results reveal that, in the nondissipative regime, regular oscillations gradually tend to chaotic with the increase of the trap asymmetry, the long-term localization disappears, and short-term localization can be changed from one of the Bose-Einstein condensates to the other through the route of Rabi oscillation. But in the dissipative regime, stationary chaos disappears and transient chaos is a common phenomenon before the regular stable frequency-locked oscillations, and a proper damping can keep the localization long lived.

DOI: 10.1103/PhysRevA.64.053604

PACS number(s): 03.75.Fi, 05.30.Jp

## I. INTRODUCTION

The macroscopic quantum property of weakly interacting Bose-Einstein condensates (BEC) has stimulated much interest for investigation of coupled BEC's. The Josephson effect, both interference and tunneling dynamics, of two-state systems is one of the hotspots [1–10]. Leggett classified it into two different types, external and internal Josephson effects. The former has two spatially separated single-particle states in a double-well trap potential, and the latter has two hyperfine internal states in a single-well trap potential [1]. The strong squeezing of the atomic number difference and a regime of squeezing in the relative phase were revealed [2,10]. Williams *et al.* demonstrated the existence of Josephson coupling for a driven two-state single-particle BEC in a single-well trap potential [9]. Smerzi *et al.* studied the coherent atomic tunneling and oscillations between two zero-temperature BEC's confined in a double-well magnetic trap [4–6,8]. The macroscopic quantum self-trapping (MQST), namely, a self-maintained population imbalance with non-zero average value of the fractional population imbalance, and the  $\pi$ -phase oscillations in which the time-averaged value of the phase difference is equal to  $\pi$  were detailed [4,5]. They claimed that the damping decays all different oscillations to the zero-phase mode [6]. In addition, macroscopic quantum fluctuations have also been discussed by using second-quantization approaches [8].

When the trapping potential is time dependent and the damping and finite-temperature effects cannot be neglected, chaos emerges. Abdullaev and Kraenkel treat the nonlinear resonances and chaotic oscillations of the fractional imbalance between two coupled BEC's in a double-well trap with a time-dependent tunneling amplitude for different dampings [11]. They also considered the chaotic atomic population resonances and the possibility of stabilization of the unstable-mode regime in coupled BEC's with oscillating

atomic scattering length [12]. Experimentally, the laser barrier position and the intensity and detuning of the laser beam in the trap can be modified, so the trap asymmetry and the amplitude of the tunneling between the coupled BEC's can be time dependent [1,4,5]; and the damping cannot be neglected [11]. Taking account of these effects, what is the route to chaos about? And when chaos appears, is the localization (i.e., the MQST) maintained or destroyed? These are still open problems, which will be discussed in this paper.

Below, we shall analyze the frequency-locked and chaotic oscillations of the fractional atomic population imbalance between two Josephson-coupled states of a two-state single-particle BEC in a time-dependent asymmetric trapping potential with damping. The outline of this paper is as follows. In the next section, the chaotic atomic population oscillations close to the separatrix solution with small trap asymmetry are analyzed by using our direct perturbation method [13–15]. The chaotic and frequency-locked population oscillations are numerically simulated in Sec. III. In the last section, the brief summary and discussion are presented.

## II. CHAOTIC ATOMIC POPULATION OSCILLATIONS CLOSE TO THE SEPARATRIX SOLUTION WITH SMALL TRAP ASYMMETRY

Within the mean-field approximation of the two-mode Gross-Pitaevskii equation, ignoring the damping and finite-temperature effects, two Josephson-coupled states of a two-state single-particle BEC are described by the nonlinear equations [2–10]

$$i\hbar \frac{\partial \psi_1}{\partial t} = [E_1 + U_1 |\psi_1|^2] \psi_1 - K \psi_2, \quad (1)$$

$$i\hbar \frac{\partial \psi_2}{\partial t} = [E_2 + U_2 |\psi_2|^2] \psi_2 - K \psi_1. \quad (2)$$

Here,  $E_1$  and  $E_2$  are zero-point energies for each condensate;  $U_1$  and  $U_2$  are proportional to the mean-field energies; and  $K$  describes the tunneling dynamics between two condensates.

\*Email address: Chlee@wipm.whcnc.ac.cn

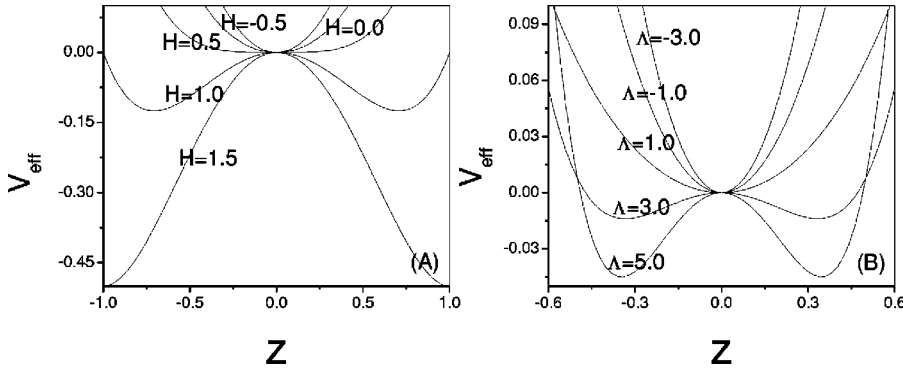


FIG. 1. The changing of the shape of the effective potential  $V_{eff}$  versus the fractional population imbalance  $z$ , (A) with  $\Lambda = 2.0$  and different  $H$ , (B) with  $H = 0.5$  and different  $\Lambda$ .

The wave functions  $\psi_i (i=1,2)$  are in the form of  $\psi_i = \sqrt{N_i(t)} \exp[i\theta_i(t)]$ , where  $N_i(t) = |\psi_i|^2$  and  $\theta_i(t)$  are the numbers of condensed atoms and phases of states. The total number of atoms  $N_T = N_1(t) + N_2(t)$  is conserved. For a time-independent parameter  $K$ , defining the fractional population imbalance  $z(t) = [N_1(t) - N_2(t)]/N_T$  and the relative phase  $\phi(t) = \theta_2(t) - \theta_1(t)$ , and scaling the time in  $2K/\hbar$ , then they obey the following differential equations

$$\frac{dz}{dt} = f(z, \phi) = -\sqrt{1-z^2} \sin \phi, \quad (3)$$

$$\frac{d\phi}{dt} = g(z, \phi) = \Delta E + \Lambda z + \frac{z}{\sqrt{1-z^2}} \cos \phi. \quad (4)$$

The parameters trap asymmetry  $\Delta E$  and atomic scattering length  $\Lambda$  determine the dynamic regimes of the BEC atomic tunneling and they can be expressed as  $\Delta E = (E_1 - E_2)/(2K) + (U_1 - U_2)N_T/(4K)$  and  $\Lambda = (U_1 + U_2)N_T/(4K)$ . The above equations indicate that  $z$  is the conjugate momentum for the generalized angular coordinate  $\phi$ , and the corresponding oscillation is the same as a non-rigid pendulum with Hamiltonian

$$H = \frac{\Lambda z^2}{2} + \Delta E z - \sqrt{1-z^2} \cos \phi. \quad (5)$$

For a time-independent trapping potential, the quasienergy of the above system is conservative. The second-order derivative of  $z$  can be derived from Eqs. (3)–(5) as

$$\begin{aligned} \frac{d^2 z}{dt^2} &= \frac{\partial f(z, \phi)}{\partial z} \frac{dz}{dt} + \frac{\partial f(z, \phi)}{\partial \phi} \frac{d\phi}{dt} \\ &= (\Lambda H - 1)z - \frac{\Lambda^2}{2} z^3 + h(t), \\ h(t) &= \Delta E H - \frac{3}{2} \Delta E \Lambda z^2 - \Delta E^2 z. \end{aligned} \quad (6)$$

Obviously, the above equation is a perturbed Duffing equation. Regarding  $z$  and  $dz/dt$  as the coordinate and momentum of an effective classical particle, respectively, its effective potential reads as

$$\begin{aligned} V_{eff} &= - \int \frac{dz}{dt^2} dz \\ &= \frac{1}{2} z^2 \left( 1 - \Lambda H + \frac{1}{4} \Lambda^2 z^2 \right) \\ &\quad + \left( \frac{1}{2} \Delta E \Lambda z^3 + \frac{1}{2} \Delta E^2 z^2 - \Delta E H z \right). \end{aligned} \quad (7)$$

If  $\Delta E = 0$ , the effective potential changes from a double well to a parabolic when increasing the value of  $(1 - \Lambda H)$  from negative to positive. The effective particle moves between the classical turning points where its kinetic energy is zero. Figure 1 shows the changing of shape of the effective potential, (A) for different values of  $H$  with a fixed value of  $\Lambda$ , and (B) for different values of  $\Lambda$  with a fixed value of  $H$ .

The motion in the parabolic potential is a Rabi oscillation with a zero time-average value of  $z$ . For fixed parameters  $\Lambda$  and  $H$ , the oscillations with small effective energies  $H_{eff} = \frac{1}{2} (dz/dt)^2 + V_{eff}$  are sinusoidal, and increasing the effective energies will add higher harmonics to the sinusoidal oscillations. In the case of double-well potential, the motion is very different from the case of the parabolic potential. When  $H_{eff} > 0$ , the motion is a nonlinear Rabi oscillation with a zero time-average value of  $z$ , which corresponds to the periodic flux of atoms from one BEC to the other. When  $H_{eff} < 0$ , the particle is confined in one of the two wells, this means the localization of atomic population in one of the two condensate states, and this localizing phenomenon has been named as macroscopic quantum self-trapping (MQST). When  $H_{eff} = 0$ , it corresponds to the threshold motion separating the above two regimes, the separatrix solution for the right-hand side well is

$$z_s(t) = 2 \sqrt{(\Lambda H - 1)/\Lambda^2} \operatorname{sech} \xi, \quad \xi = C_0 + t \sqrt{\Lambda H - 1}. \quad (8)$$

Here, constant  $C_0 = \operatorname{Ar} \operatorname{sech}\{z_s(0)/[2 \sqrt{(\Lambda H - 1)/\Lambda^2}]\}$ .

The dynamics of the fractional population imbalance near the separatrix solution sensitively depends on the initial conditions and system parameters such that it becomes chaotic with a stochastic layer. The Melnikov function method is useful to find the regions of chaotic oscillation [11,12]. Based upon our understanding of the chaotic dynamics of the perturbed pendulum and rf-driven superconducting Joseph-

son junction [13,14], we will use our direct perturbation approaches to analyze the stability of the boson Josephson junction in the following.

Now we take into account the damping effects. For two coupled BEC's in a double-well potential with a noncoherent dissipative current of normal-state atoms, the damping term of Eq. (3) is  $-\eta d\phi/dt$ ; and for two interacting condensates with different hyperfine levels in a single-well potential, the damping has the form  $-\eta z(t)$  (i.e., the damping term in the right of Eq. (6) is  $-\eta dz/dt$ ) [9,11,12]. In this paper, we only consider the latter case. When the trap asymmetry and damping amplitude is very small, they can be treated as perturbations to the symmetric system ( $\Delta E=0$ ). Then the function  $h(t)$  becomes

$$h(t) = \Delta EH - \frac{3}{2} \Delta E \Lambda z^2 - \Delta E^2 z - \eta \frac{dz}{dt}. \quad (9)$$

In addition to a time-independent trap asymmetry  $\Delta E_0$ , we impose a sinusoidal variation, so the asymmetry  $\Delta E = \Delta E_0 + \Delta E_1 \sin \omega t$ ; this can be realized by varying the laser barrier position or detuning of the laser beam [1,4,5]. According to our analytical approach [13,14], if the trap asymmetry and the damping amplitude satisfy

$$\Delta E = \varepsilon(\Delta E_0 + \Delta E_1 \sin \omega t), \quad \eta = \varepsilon \eta', \quad |\varepsilon| \ll 1, \quad (10)$$

the solution close to the separatrix solution may be expressed as

$$z = \sum_{i=0}^{+\infty} \varepsilon^i z_i = z_0 + \varepsilon z_1 + \varepsilon^2 z_2 + \dots \quad (11)$$

Here,  $z_i$  are the  $i$ th order corrections. Substituting the above expression into Eq. (6) and comparing the coefficient function of every  $\varepsilon^i$  for both sides of the differential equation, we obtain  $z_i$  satisfy the equations

$$\frac{d^2 z_0}{dt^2} - (\Lambda H - 1) z_0 + \frac{\Lambda^2}{2} z_0^3 = 0. \quad (12)$$

$$\frac{d^2 z_i}{dt^2} - (\Lambda H - 1) z_i + \frac{3\Lambda^2}{2} z_0^2 z_i = \epsilon_i, \quad (i = 1, 2, 3, \dots), \quad (13)$$

with

$$\begin{aligned} \epsilon_1 &= -\eta' \frac{dz_0}{dt} + \Delta EH - \frac{3}{2} \Delta E \Lambda z_0^2, \\ \epsilon_2 &= -\eta' \frac{dz_1}{dt} - 3\Delta E \Lambda z_0 z_1 - \frac{3}{2} \Lambda^2 z_0 z_1^2 - \Delta E^2 z_0, \\ &\dots \end{aligned}$$

We take the zero-order solution as the separatrix solution  $z_0 = z_s$  of Eq. (8), and the basic solutions of the unperturbed high-order equations (13) with ( $\epsilon_i = 0$ ) are as follows

$$z_{i1}^0 = \frac{dz_0}{dt} = -\frac{2(\Lambda H - 1)}{\sqrt{\Lambda^2}} \operatorname{sech} \xi \tanh \xi. \quad (14)$$

$$\begin{aligned} z_{i2}^0 &= z_{i1}^0 \int (z_{i1}^0)^{-2} dt \\ &= \frac{-\sqrt{\Lambda^2}}{16(\Lambda H - 1)^{3/2}} \operatorname{sech}^2 \xi (\cosh 3\xi - 9 \cosh \xi \\ &\quad + 12\xi \sinh \xi). \end{aligned} \quad (15)$$

So the general expressions of  $i$ th corrections are

$$z_i = z_{i2}^0 \int_{C_1}^t z_{i1}^0 \epsilon_i dt - z_{i1}^0 \int_{C_2}^t z_{i2}^0 \epsilon_i dt. \quad (16)$$

Constants  $C_1$  and  $C_2$  are determined by the initial conditions and the physical parameters. When time  $t \rightarrow \pm\infty$ , Eqs. (14) and (15) give  $|z_{i1}^0| \rightarrow 0$  and  $|z_{i2}^0| \rightarrow +\infty$ . Solving the  $i$ th order equations one by one, we can obtain functions  $\epsilon_i$  containing time-periodic functions with finite amplitudes. This means the high-order corrections are unbounded unless the coefficient functions of the growing function  $z_{i2}^0$  vanish at  $t = \infty$ . So the general motion is unstable oscillations, the necessary-sufficient conditions for bounded oscillations are expressed as

$$\lim_{t \rightarrow \pm\infty} \int_{C_1}^t z_{i1}^0 \epsilon_i dt = 0. \quad (17)$$

The boundedness of perturbed corrections means stability of the system under deterministic perturbation. Here, and throughout the paper, the stable chaos is defined for the deterministic perturbation without any random disturbance. Although the above conditions are nonintegrable, they contain the integrable necessary conditions

$$\int_{-\infty}^{+\infty} z_{i1}^0 \epsilon_i dt = 0. \quad (18)$$

The first-order integration ( $i = 1$ ) is the Melnikov function of the system, which equates zero, indicating the existence of Melnikov chaos. This implies that the stable oscillations are chaotic, but not all chaotic oscillations are stable because of the nonsufficient property of the condition (18). Integrating the above equations, one may evidence the necessary conditions as a series of relations of the initial conditions and parameters. For fixed initial conditions, modifying the parameters may control the instability of the chaotic oscillations. Substituting the expressions of  $z_{i1}^0$  and  $\epsilon_1$  into Eq. (18) and integrating it yield the first-order condition

$$\begin{aligned} & -\frac{8\eta'(\Lambda H - 1)\sqrt{\Lambda H - 1}}{3\Lambda^2} - \frac{2\Delta E_1 H}{\sqrt{\Lambda^2}} \\ & \times \omega \pi \cos \frac{\omega C_0}{\sqrt{\Lambda H - 1}} \operatorname{sech} \frac{\omega \pi}{2\sqrt{\Lambda H - 1}} \end{aligned}$$

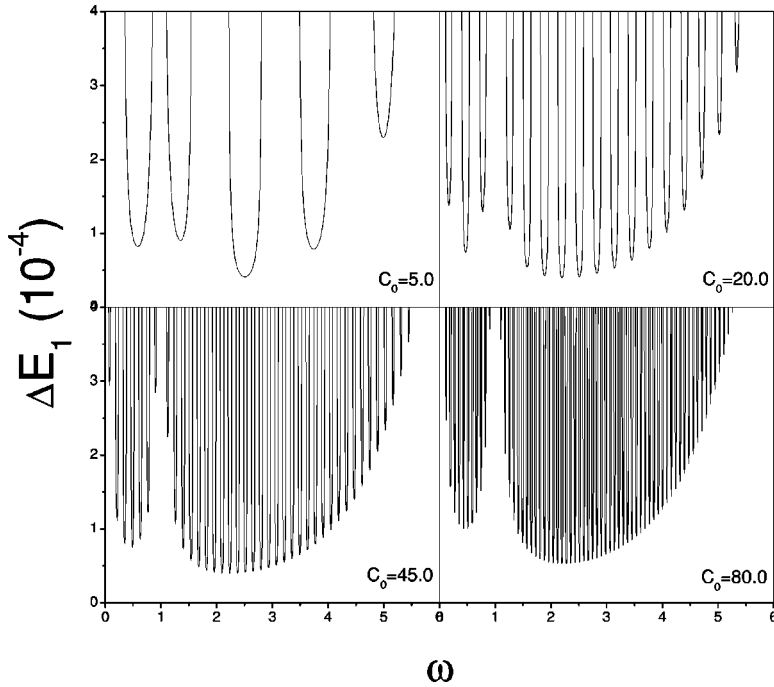


FIG. 2. The stability curves for different initial conditions with  $H=0.5$ ,  $\Lambda=0.5$ ,  $\Delta E_0=0.0$ , and  $\eta'=0.5 \times 10^{-4}$ .

$$+ \frac{2\Delta E_1(\Lambda H - 1)\sqrt{\Lambda H - 1}}{\Lambda\sqrt{\Lambda^2}} \left(1 + \frac{\omega^2}{\Lambda H - 1}\right) \times \omega \pi \cos \frac{\omega C_0}{\sqrt{\Lambda H - 1}} \operatorname{sech} \frac{\omega \pi}{2\sqrt{\Lambda H - 1}} = 0. \quad (19)$$

The independence of the above-necessary condition on the time-independent trap asymmetry  $\Delta E_0$  means that the chaotic oscillations are caused by the time-dependent trap asymmetry. However, this does not imply that the stability is irrelevant to the time-independent trap asymmetry, since the sufficient-necessary conditions (17) and high-order necessary conditions (18) with  $i > 1$  are correlated with  $\Delta E_0$  and other parameters. For the same parameters, the distribution of stability curves sensitively depends on the initial conditions. To display this dependence explicitly, we have chosen a series of values of the initial constant  $C_0$  to plot Fig. 2 from Eq. (19), in which the curves become denser and denser with the growing of the value  $C_0$ ; this illustrates the existence of chaos. The transition between the regular oscillations and the chaotic ones is described by the curves shown in Fig. 3. Regions above the curves correspond to Melnikov chaotic oscillations of the fractional population imbalance and those below correspond to the regular oscillations. There exist two chaotic regions separated by a special frequency that is determined by the physical parameters, and this frequency may cause an unstable nonlinear resonance. When the damping becomes stronger and stronger, the regions of chaotic oscillations become smaller and smaller, and the regular region becomes larger and larger.

### III. NUMERICAL SIMULATION OF CHAOTIC AND FREQUENCY-LOCKED ATOMIC POPULATION OSCILLATIONS

When the atomic population oscillations are far away from the separatrix solution, or when the trap asymmetry and

the damping are large enough, the oscillating dynamics cannot be obtained from the previous analytical method. In this section, by numerically integrating Eqs. (3) and (4) with the fourth Runge-Kutta method with variable step widths, we simulate the atomic population oscillations that has fixed coupling  $K$ , and time-dependent trap asymmetry  $\Delta E = \varepsilon(\Delta E_0 + \Delta E_1 \sin \omega t)$  and damping term  $-\varepsilon \eta' z(t)$  in the right side of Eq. (3).

In the case of the time-independent symmetric trap potential ( $\Delta E = 0$ ), because of the damping, both Rabi oscillation and MQST reach an equilibrium state with zero population imbalance, see Figs. 4(b) and (f); increasing the trap asymmetry ( $\Delta E$ ) to 1.0 leads to the departure of the equilibrium state from zero population imbalance, see (d) and (h) of Fig. 4. Ignoring the damping effects, the oscillations are regular, they contain two different kinds, Rabi oscillation and MQST, see (a), (e), (c), and (g) of Fig. 4.

In the case of the time-dependent asymmetric trap poten-

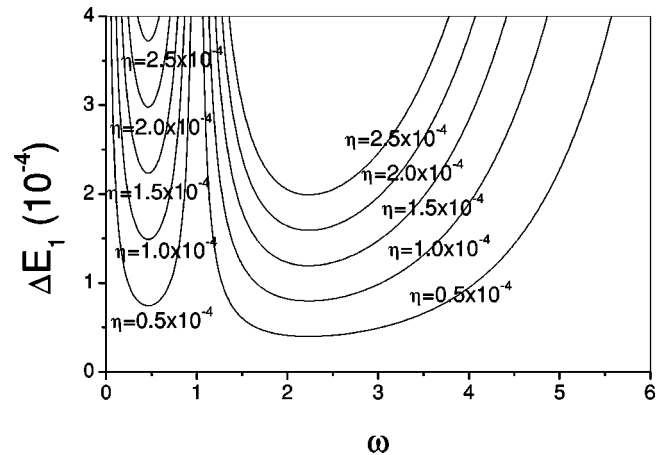


FIG. 3. The regions of chaotic oscillations for different values of the damping parameter  $\eta'$ , with  $\Lambda=4.0$ ,  $\Delta E_0=0$ , and  $H=0.5$ .



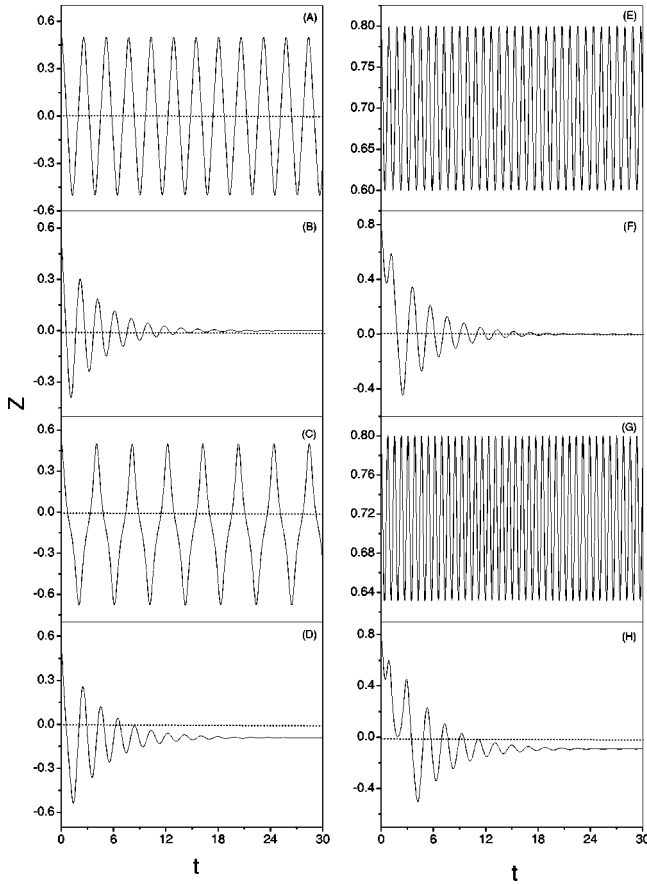


FIG. 4. The time evolution of the fractional population imbalance  $z$  with  $\Lambda=10$ , the left column with initial conditions  $z(0)=0.5$  and  $\phi(0)=0.0$ , the right column with  $z(0)=0.8$ ,  $\phi(0)=0.0$ . (A) and (E) with  $\Delta E=0.0$  and  $\eta'=0.0$ ; (B) and (F) with  $\Delta E=0.0$  and  $\eta'=0.5$ ; (C) and (G) with  $\Delta E=1.0$  and  $\eta'=0.0$ ; (D) and (H) with  $\Delta E=1.0$  and  $\eta'=0.5$ .

tial ( $\Delta E_1 \neq 0$ ), the chaotic oscillation appears. For simplicity, we choose  $\Delta E_0=0$ , the dimensionless parameter  $\varepsilon=1$ , the initial phase  $\phi(0)=0$ , and the atomic scattering length  $\Lambda=10$ . Sampling a single trajectory once within every period of the variation of the trap asymmetry, we obtain the stroboscopic Poincare section. In the nondissipative regime ( $\eta'=0$ ), with the increase of the time-dependent trap asymmetry  $\Delta E_1$ , the sections vary from a single island to a lot of islands, and all islands are finally submerged by the chaotic sea. This means the periodic oscillations change into quasi-periodic, and then chaotic. Figure 5 is the Poincare sections of  $(z, dz/dt)$ , with the initial conditions  $z(0)=0.5$ , the parameters  $\omega=4\pi$ , and different values of  $\Delta E_1$ , the corresponding oscillation in its beginning is a Rabi oscillation. When  $\Delta E_1=3.000$ , there is only a single island. Then it is separated into six islands as  $\Delta E_1$  increase to 6.000. For larger trap asymmetry  $\Delta E_1=6.750$ , the regular islands are surrounded by the chaotic sea. For large enough trap asymmetry  $\Delta E_1=7.500$ , the regular islands are all submerged by the chaotic sea, and the sea is symmetrical with zero time-averaged value of  $z$ . Evolving from a MQST, the Poincare sections with  $z(0)=0.75$ ,  $\omega=2\pi$ , and different values of  $\Delta E_1$  is showed in Fig. 6, where the similar chaotic dynamics

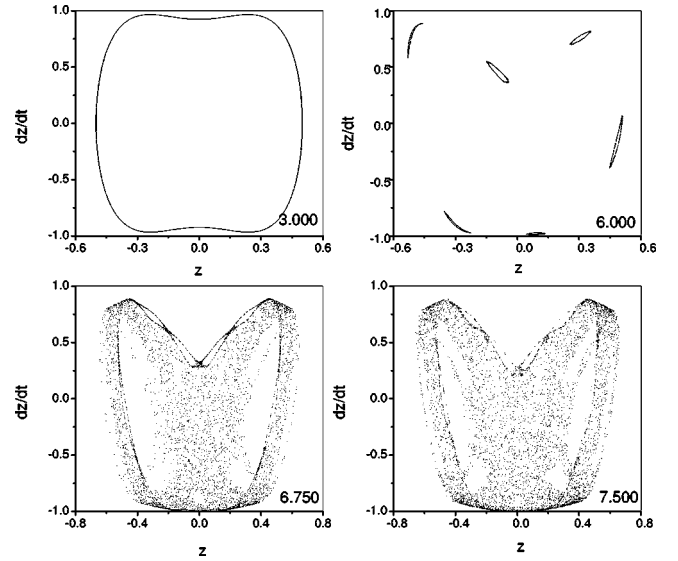


FIG. 5. The stroboscopic Poincare sections of  $(z, dz/dt)$  in the nondissipative regime with  $z(0)=0.5$ ,  $\omega=4\pi$  and different values of  $\Delta E_1$ .

is exhibited. For small  $\Delta E_1$  (1.000, 1.560, and 1.565), the time-averaged value of the fractional population imbalance is nonzero, and the atoms are localized on one of the condensates. However, for large enough  $\Delta E_1$  (1.700), the chaotic sea is also symmetrical to the line  $z=0$ . This indicates that, in the completely chaotic oscillation, the time-averaged value of the fractional population imbalance is zero, and the long-lived MQST or localization disappears.

The completely chaotic oscillations of the fractional population imbalance evolving from Rabi oscillation and MQST are presented in Fig. 7. The left column corresponds to  $z(0)=0.5$ ,  $\omega=4\pi$ , and  $\Delta E_1=7.500$ ; the right column corresponds to  $z(0)=0.75$ ,  $\omega=2\pi$ , and  $\Delta E_1=1.700$ . The

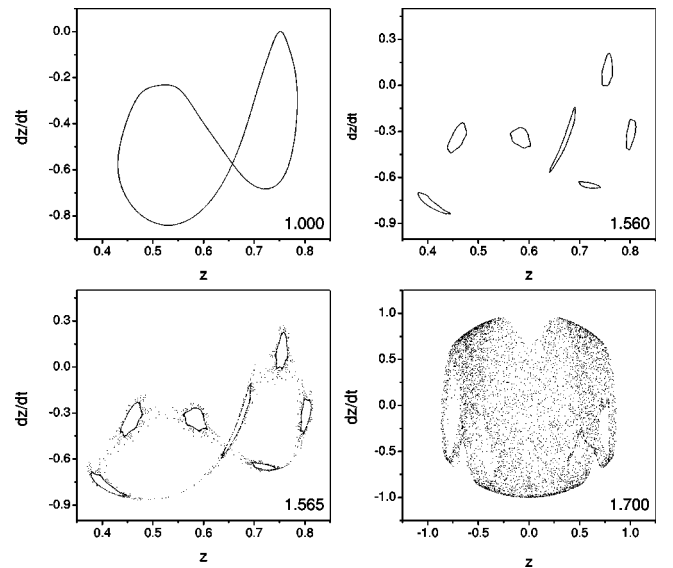


FIG. 6. The stroboscopic Poincare sections of  $(z, dz/dt)$  in the nondissipative regime with  $z(0)=0.75$ ,  $\omega=2\pi$  and different values of  $\Delta E_1$ .

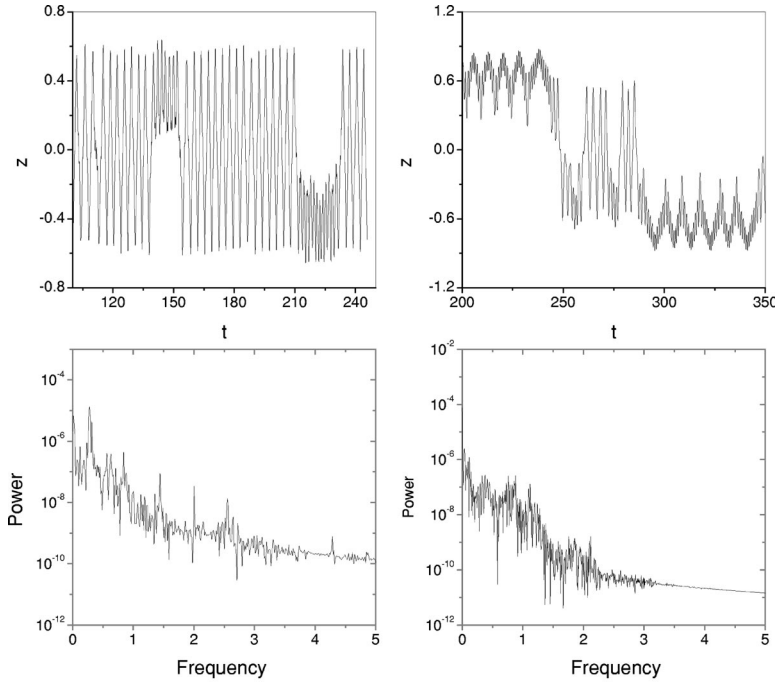


FIG. 7. The completely chaotic oscillations and the corresponding power spectra in the non-dissipative regime. The left column corresponds to  $z(0)=0.5$ ,  $\omega=4\pi$ , and  $\Delta E_1=7.500$ . The right column corresponds to  $z(0)=0.75$ ,  $\omega=2\pi$ , and  $\Delta E_1=1.700$ .

first row is the time evolution of  $z$ , the second row is the power spectra of the corresponding oscillation. Clearly, through the route of Rabi oscillation, the short-term localization or MQST can be changed from one of the BEC's to the other, and the corresponding power spectra is very noisy.

In the dissipative regime ( $\eta' \neq 0$ ), because of the existence of the damping effects, the volume in phase space will decrease through time evolution. A common phenomenon in these dynamical systems is that they seem to behave chaotically during some transient periods, but eventually fall onto periodic stable attractors. This is known as the transient chaos or chaotic transient. Superlong transient chaos occurs commonly in dissipative dynamical systems, where oscillations that start from arbitrary initial conditions oscillate chaotically for a very long time before they set into the final attractors, which are usually regular and stable [16,17]. In our two-state BEC system, we also find transient chaos and final attractors. We will exhibit the attracting process of the transient chaos and the fixed points of the final attractors in the Poincare sections of  $(z, dz/dt)$ . The phase trajectories of the final attractors are also shown.

For a fixed value of damping amplitude  $\eta'$ , there exist many types of attractors when  $\Delta E_1$  is changed. Fixing the  $\Delta E_1$ , different initial conditions will lead to different final states. Starting from a Rabi oscillation, with  $z(0)=0.5$ ,  $\omega=4\pi$ ,  $\eta'=0.01$ , and different values of  $\Delta E_1$ , the Poincare sections of the attracting processes and the final attractors, and the phase trajectories of the final attractors are presented in Fig. 8. The left column shows the Poincare sections of the attracting processes; the right column shows the phase trajectories and Poincare sections of the final states, (a) and (b) for  $\Delta E_1=3.000$ , (c) and (d) for  $\Delta E_1=7.500$ . In the Poincare sections, after the transient chaos, the sampled points gradually approach the final fixed points. The phase trajectories of final oscillations are closed curves, and the corresponding Poincare sections only contain fixed points that are denoted

as small circles, so that the final oscillations are frequency locked (FL). When  $\Delta E_1=3.000$ , there is only a single fixed point in the Poincare sections, the corresponding final oscillation is a period-one limit-cycle with frequency  $\omega$ . While for  $\Delta E_1=7.500$ , there exist five fixed points, and then the final oscillation is a 1/5 FL motion, this means the oscillating frequency is  $(1/5)\omega$ . Figure 9 presents similar dynamics evolving from a MQST with  $z(0)=0.75$ ,  $\omega=2\pi$ , and  $\eta'=0.001$  for different parameter  $\Delta E_1$ . Where, (a) and (b) for  $\Delta E_1=1.000$ , (c) and (d) for  $\Delta E_1=1.700$ . The transient chaos and the FL oscillations appear too. When  $\Delta E_1=1.000$ , the eventual oscillation is a period-one limit cycle

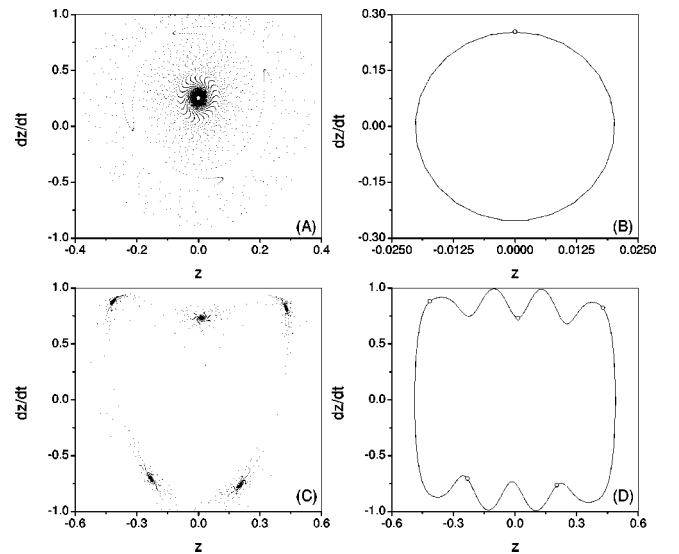


FIG. 8. The stroboscopic Poincare sections of  $(z, dz/dt)$  in dissipative regime and frequency-locked oscillations with  $z(0)=0.5$ ,  $\eta'=0.01$ , and different values of  $\Delta E_1$ . (A) and (B) with  $\Delta E_1=3.000$ , (C) and (D) with  $\Delta E_1=7.500$ .

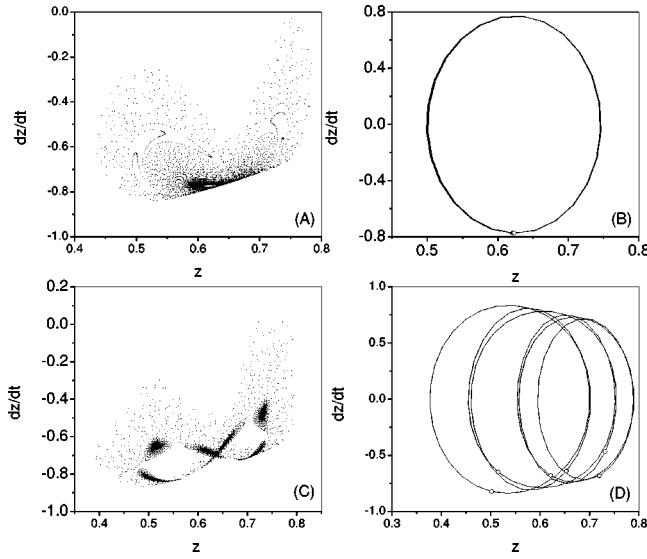


FIG. 9. The stroboscopic Poincaré sections of  $(z, dz/dt)$  in dissipative regime and frequency-locked oscillations with  $z(0) = 0.75$ ,  $\omega = 2\pi$ ,  $\eta' = 0.001$ , and different values of  $\Delta E_1$ . (A) and (B) with  $\Delta E_1 = 1.000$ , (C) and (D) with  $\Delta E_1 = 1.700$ .

with a nonzero time-averaged value of the fractional population imbalance  $z$ , so the atoms are localized on one of the condensates. Amazingly, for large  $\Delta E_1$  (1.700), due to the damping effects, the final 1/6 FL oscillation possesses a nonzero time-averaged value of  $z$ . Comparing with the non-damping regime (Fig. 6), one can see that a proper damping can keep the MQST long lived.

#### IV. SUMMARY AND DISCUSSIONS

With both analytical and numerical methods, we have studied the chaotic and frequency-locked oscillations between two coupled Bose-Einstein condensates in a time-dependent asymmetric trap potential. The trap asymmetry has been chosen as Eq. (10), which can be realized by varying the laser barrier position or the detuning of the laser beam [1,4,5]. The damping of the oscillations of the fractional population imbalance is taken as the form  $-\eta z(t)$ , it commonly exists in two interacting condensates with two different hyperfine levels in a single-well trapping potential [11,12].

In the perturbative regime, the population oscillations have been depicted with the Duffing equation, and the chaotic oscillations near the separatrix solution are detailed. In this regime, the Melnikov function approach is a valid way to predict the onset of chaos in the population oscillations that are close to the separatrix. Using this method, Abdullaev and Kraenkel analyzed the population oscillations of two coupled BEC's with time-dependent coupling [11] and oscillating atomic scattering length [12], and gave out the criteria for the onset of chaos. In this article, based on our successful

analysis of perturbed pendulum [13] and superconducting Josephson junction [14], we have discussed the stability of the population oscillations near the separatrix by using the direct perturbation technique. A formally general solution of the perturbed system gave the correction to the separatrix solution. Theoretical analysis revealed that the sufficient-necessary conditions for bound oscillations contain Melnikov criterion for chaos. This indicates that the bounded oscillations are embedded in a chaotic attractor. The boundedness conditions imply the sensitive dependence of the system on initial conditions. The regions of chaotic and regular oscillations can be exchanged by varying the damping strength.

However, when the oscillations are not close to the separatrix solution, and the system parameters are not in perturbative regime, the numerical method is unavoidable. The chaotic population and frequency-locked oscillations are simulated by straightforward numerical integration of the motion equations. In the nondissipative regime, regular oscillations gradually tend to become chaotic ones with the increased values of  $\Delta E_1$ . In the case of completely chaotic oscillations, the long-lived localizations or MQST's are completely destroyed, and the short-term localization or MQST can be exchanged from one of the BEC's to the other through the route of the Rabi oscillation. In the corresponding Poincaré section, the single regular island is separated into many small islands, and all islands are finally submerged into the chaotic sea. In the dissipative regime, due to the damping effects, the volume of the phase space is reduced by time evolution. Then the stationary chaos disappears, and transient chaos is a common phenomenon before becoming regular, stable frequency-locked oscillations. Surprisingly, a proper damping strength can keep the localization or MQST long lived.

Experimentally, the long-term average lifetime of the transient chaotic oscillation requires long-term measurements, too. So the prediction of the relation between the average lifetime of the transient and the physical parameters ( $\eta$ ,  $\Delta E_0$ ,  $\Delta E_1$ , and  $\Lambda$ ) may be a practical problem. And if one wants to observe the long-lived localization or MQST, understanding attraction basins of the eventual frequency-locked oscillations in parameter space will give some useful indication for how to choose the physical parameters. These results will be reported elsewhere.

#### ACKNOWLEDGMENTS

The work was supported by the National Natural Science Foundations of China under Grant Nos. 19734060, 19874019, 19904013, and 1990414. The authors are very grateful for the help of Professor Wing-Ki Liu (Department of Physics, University of Waterloo, Canada), Professor Hugh Klein (National Physical Laboratory of United Kingdom), Professor Yiwu Duan, Dr. Mang Feng, Dr. Haoseng Zeng, and Dr. Zongxiu Nie.

- [1] A.J. Leggett, Rev. Mod. Phys. **73**, 307 (2001).
- [2] M.J. Steel and M.J. Collett, Phys. Rev. A **57**, 2920 (1998).
- [3] Chi-Yong Lin and E.J.V. de Passos, Phys. Rev. A **62**, 055603 (2000).
- [4] A. Smerzi, S. Fantoni, S. Giovanzzi, and S.R. Shenoy, Phys. Rev. Lett. **79**, 4950 (1997).
- [5] S. Raghavan, A. Smerzi, S. Fantoni, and S.R. Shenoy, Phys. Rev. A **59**, 620 (1999).
- [6] I. Marino, S. Raghavan, S. Fantoni, S.R. Shenoy, and A. Smerzi, Phys. Rev. A **60**, 487 (1999).
- [7] I. Zapata and F. Sols, Phys. Rev. A **57**, R28 (1998).
- [8] A. Smerzi and S. Raghavan, Phys. Rev. A **61**, 063601 (2000).
- [9] J. Williams *et al.*, Phys. Rev. A **59**, R31 (1999).
- [10] C. Orzel *et al.*, Science **291**, 2386 (2001).
- [11] F.Kh. Abdullaev and R.A. Kraenkel, Phys. Rev. A **62**, 023613 (2000).
- [12] F.Kh. Abdullaev and R.A. Kraenkel, arXiv: e-print cond-mat/0005445 (2000).
- [13] Wenhua Hai *et al.*, Phys. Lett. A **275**, 54 (2000).
- [14] Wenhua Hai *et al.*, Phys. Lett. A **265**, 128 (2000).
- [15] Chaohong Lee *et al.*, Acta Phys. Sin. **47**, 1409 (1998).
- [16] J. Hoffnagle and R.G. Brewer, Science **265**, 213 (1994); Phys. Rev. Lett. **71**, 1828 (1993); Phys. Rev. A **50**, 4157 (1994).
- [17] Jing-Ling Shen, Hua-Wei Yin, and Jian-Hua Dai, Phys. Rev. A **55**, 2159 (1997).